NUMERICAL SIMULATION OF NEAR-SHORE WAVE BREAKING USING SPH METHOD

Christos V. Makris[1], Constantine D. Memos[2] and Yannis N. Krestenitis[1]

Abstract: Wave breaking over relatively mild sloping beaches is discussed in this paper. Experimental and numerical aspects are investigated and comparisons between results are pursued. In this framework, a modern promisingly efficient method called Smoothed Particle Hydrodynamics is used and the academic 'open source' code SPHysics is being validated against experimental data. Moreover, an attempt is made to verify its ability to capture the dynamics of near-shore wave breaking features and the characteristics of surf and swash zone turbulence. Drawbacks of the model are pin-pointed and specific improvements are proposed for future research.

INTRODUCTION

Near-shore wave propagation, shoaling and depth related breaking are three of the most significant coastal processes. Especially the latter is a parameter of major importance in assessing the surf and swash zone wave pattern, quantifying the near-shore velocities and describing the coherent turbulent structures (cts), which primarily control sediment movements and cross-shore morphodynamic evolution. In this direction, modern research focuses upon the derivation of instantaneous and phase-averaged values of quantities, such as vorticity ω, fluctuating turbulent components of velocity u' & w' ($u = \bar{u}+u'$, u = fluid velocity, $\bar{u}$ = time-average velocity component), turbulent kinetic energy $k = [u'^2+w'^2]/2$, turbulent shear and normal stresses $\tau' = u'w'$, $\sigma' = u'^2$ or w'^2, turbulence production Pr, distances between vortices, characteristic inertial and dissipative length and time scales etc. Moreover, the conceptual design of modern coastal protection works requires nowadays, except from the wave height H and free-surface elevation η, the exact representation of deformed free surface due to breaking, undertow U, wave setup SU, run-up RU and overtopping not thoroughly

1 Aristotle University of Thessaloniki, Enginnering Faculty, Civil Engineering Department, Division of Hydraulics and Environmental Engineering, Laboratory of Maritime Engineering and Maritime Works, GR54124 – Thessaloniki (Greece) cmakris@civil.auth.gr, ynkrest@civil.auth.gr

2 National Technical University of Athens, School of Civil Engineering, Laboratory of Harbour Works, Heroon Polytechniou 5, GR15780, Zografos – Athens (Greece) memos@hydro.ntua.gr

provided by classical analytical theories or numerical wave propagation models, like Boussinesq and mild-slope equation ones.

Quantification measures of the aforementioned processes have been extensively provided throughout the last decades by various laboratory experiments, which involve physical modelling of wave generation, propagation and breaking of the spilling or plunging type, on inclined beach slopes placed inside small scale wave flumes. These efforts are several and mostly account for linear and non-linear regular and solitary waves propagating and breaking on relatively mild slopes. The methods implemented, vary from the early photographic capturing of the breaking wave process with simultaneous measurements of the free surface at specific gauge points throughout the propagation, surf and swash zone regions to the more elaborate modern Acoustic/Laser Doppler Velocimetry (ADV/LDV) or Anemometry (LDA), e.g. those used by Nadaoka et al. (1989) and more recent researchers presented below. Furthermore Particle Image Velocimetry (PIV) methods (Grue et al., 2004) are frequently used nowadays, covering broader areas than gauges and record high frequency frames of the flow field, thus depicting its overall turbulent patterns and structures. Extended and thorough reviews on the matter can be found in the works of Longo et al. (2002) and Christensen (2006), while Elfrink & Baldock (2002) focus on the swash zone dynamics.

The short term goal of the present study is the exact simulation of the highly nonlinear process of wave breaking on plane and relatively mild impermeable slopes. In the long run, we aim at quantifying *U* and *RU* on sloping beaches, as well as loading and overtopping of coastal structures with steeper slopes. Followingly, one of the most recent comprehensive studies on surf zone breaking waves and consequent turbulence transport under them is presented and incorporated in the evaluation process of a numerical model implementing a modern gridless approach of discretization for the computational domain. Comparisons of the model's results are made here with the ones of the experimental setup introduced below.

SPH METHODOLOGY

Smoothed Particle Hydrodynamics (SPH) method as described by Monaghan (1994, 2005) is one of the most ingenuous modern numerical methods for the simulation of hydrodynamic free-surface flows. It is a mesh-free particle method, implementing Lagrange-type approximation for the Navier-Stokes equations, through integral interpolation smoothing functions. Its Lagrangian nature allows the unhindered simulation of free-surface flows with strong deformations, such as wave breaking (e.g. plunging) or wave-structure interaction in coastal areas, as described by Rogers & Dalrymple (2004), Dalrymple & Rogers (2006) and Crespo et al. (2007, 2008).

Thorough analysis of the SPH method can be found in Liu & Liu (2003), thus only general reference of the constitutive equations will be attempted here. The main inspiration of the method is the integral interpolation of a function $A(\mathbf{r})$, as

$$A(\mathbf{r}) = \int A(\mathbf{r}')W(\mathbf{r}-\mathbf{r}', h)d\mathbf{r}' \quad (1)$$

where h = smoothing length, $\mathbf{r}$ = arbitrary particle point, $\mathbf{r}'$ = distance between particles,

$W(\mathbf{r},h)$ = a distance varied weighting function called kernel. Please note that in bold notation are presented the vector and tensor quantities. In discrete notation Eq. 1 reads

$$A(\mathbf{r}) = \sum_b m_b \frac{A_b}{\rho_b} W_{ab} \tag{2}$$

where m_b, ρ_b mass and density of particle b respectively.

Weighting Function

A variety of weighting functions is available in the bibliography, all accounting for certain attributes, such as positivity, compact support, normalization, monotonic decreasing and delta function behaviour (for infinitely small h). A classic one with no inflection point in its derivative formula is of quadratic type, written as

$$W(\mathbf{r}_{ij}, h) = a_D \left(1 - q + q^2/4\right) \tag{3}$$

where $q = \mathbf{r}_{ij}/h$, $\alpha_D = 3/2\pi h^2$ for 2-D, $\mathbf{r}_{ij}$ = distance between particles i, j. In practice the kernel influence domain is confined in a radial distance of $2h$ and a tracking technique like 'nearest neighbour list' is used to truncate the summation in Eq. 2, thus including only the close to the point of interest neighbour particles, which actually are the spatially discretized nodes of the computational domain, to which we have attributed mass.

Continuity, Momentum and Kinematics Equations

Conservation of mass and momentum (Navier-Stokes equations) in particle formulation are written according to Monaghan (1994) as

$$\frac{d\rho_i}{dt} = \sum_j m_j \left(\mathbf{u}_i - \mathbf{u}_j\right) \cdot \nabla_i W_{ij} \tag{4}$$

$$\frac{d\mathbf{u}_i}{dt} = -\sum_j m_j \left(\frac{P_i}{\rho_i{}^2} + \frac{P_j}{\rho_j{}^2} + \Pi ij\right) \cdot \nabla_i W_{ij} + \mathbf{g} + \sum_j m_j \left(\frac{4\nu \mathbf{r}_{ij}\mathbf{u}_{ij}}{\left(\rho_i + \rho_j\right)\left|\mathbf{r}_{ij}\right|^2}\right) \nabla_i W_{ij} \tag{5}$$

where $\mathbf{u}_j$, P_j the velocity, pressure of particle j respectively, $\mathbf{g}$ = (0, 0, 9.81) m/sec^2 the gravitational acceleration, ν = 10^{-6} m^2/sec the kinematic viscosity, W_{ij} the kernel function between i particle and arbitrary surrounding ones in its influence domain, ∇_i the gradient or spatial derivative with respect to the coordinates of particle i and Π_{ij} an artificial empirical viscosity term (Monaghan, 1994):

$$\Pi_{ij} = -a\mu_{ij}\bar{c}_{ij} / \bar{\rho}_{ij} \tag{6}$$

with $\alpha = 0.01 \sim 0.1$, $\mu_{ij} = (\mathbf{u}_i - \mathbf{u}_j)\mathbf{r}_{ij}/(\mathbf{r}_{ij}{}^2 + 0.01h^2)$ and over-bared features denoting average property values between i and j particles. The latter are manipulated in such a way, that they move with approximately the same velocity as the average one of the neighbour particles, preventing them from occupying the same location with others. The relation, following the so called XSPH correction, with empirical term $\varepsilon \approx 0.5$, is

$$\frac{d\mathbf{r}_i}{dt} = \mathbf{u}_i + \varepsilon \sum_j m_j \left(\frac{\mathbf{u}_i - \mathbf{u}_j}{\bar{\rho}_i} \right) W_{ij} \tag{7}$$

Equation of State

In order to relate the pressure to the density of the fluid, the artificial compressibility concept is incorporated in compressible SPH models, providing us with the advantage of using an equation of state instead of having to solve for an extra Poisson-type equation for pressure, describing incompressible flows. Monaghan (1994), based on Batchelor (1974), provides the following expression for the particle pressure

$$P = B\left[\left(\rho / \rho_o \right)^{\gamma} - 1 \right] \tag{8}$$

where $\gamma = 7$, $B = c_o^2 \rho_o / \gamma$, reference density $\rho_o = 1000$ kgr/m^3 and speed of sound $c_o = c(\rho_o) = \partial P / \partial \rho|_{\rho o}$. By altering the B value, we can adjust the speed of sound c_s to approximately ten times the largest wave celerity c_{max} under consideration. The sound speed turns out to be much lower than its real value, yet makes computations much faster. Moreover the computational Mach number is of the order $M = c_{max}/c_s = 0.1$, which ensures that fluid density gradients are almost 1% or even less, since compressibility effects are O(M^2), following the Prandtl-Glauert rule, which relates compressible to incompressible correction factors K_c and K_i respectively as follows:

$$\frac{K_c}{K_i} = \frac{1}{\sqrt{1 - M^2}} \tag{9}$$

All in all, the verification of the capability of the various implementations of the SPH method to predict the details of the entire wave breaking process is being pursued. In this framework the academic 'open source' numerical code SPHysics (Gómez-Gesteira et al., 2007) is used. It has been developed during the last years by several researchers around the world with its origin at JHU (Baltimore, USA) and its applicability is being tested here by incorporating to the present investigation one numerical setup, simulating experiments by Stansby & Feng (2005) [S&F].

Their aim was the determination, through phase- and ensemble-averaging, of recurrent vertical flow structures, including from large-scale motions down to small-scale vertical structures. The coherent character of multiple vortical structures was confirmed, specifically just before and at the onset of breaking, giving its place to elongated ones near and along the free surface during the turbulent bore propagation. Period-averaged ω and u', w' were also obtained showing onshore mass transport above trough level and undertow-type backflow below it. Thick vorticity layers were observed at trough level and a thin one rotating oppositely near the bottom solid boundary. Various turbulence terms were evaluated, taking for granted a slow variation of space/time transformation phase speed, while the net balance values were always negligible compared to the maxima ones.

SPHYSICS MODEL IMPLEMENTATION

The basic model used in this study is presented below, along with its calibration.

Boundary Conditions

Solid boundaries inside the computational domain are treated as either dynamic or repulsive boundaries (Gómez-Gesteira et al., 2007). The first approximation assumes boundary particles fixed in a staggered way, having the properties of the fluid particles, yet with zero velocities. The second one introduces repulsive forces between fixed, co-linear solid particles and fluid ones through the use of the Lennard-Jones molecular potential. Both treatments define a more or less slip boundary condition in the inviscid limits.

Viscosity Treatment

Dalrymple and Rogers (2006) discuss the use of the artificial viscosity term (Eq. 6), which is used to keep particles from interpenetration, represent viscosity and afford numerical stability for free surface problems. Nonetheless it influences negatively the shear in the fluid, by introducing very dissipative structures in the numerical scheme, a fact specifically significant if someone tries to describe cts. In SPHysics a Sub-Particle Scale (SPS) is available for the unresolved scales, while the large-scale eddies are modelled implicitly by fine spatial resolution. A compressible fluid Favre-averaging technique, $\tilde{f} = \overline{\rho f} / \bar{\rho}$, where the overbar denotes flat-top arbitrary spatial filtering (Rogers & Dalrymple, 2004), is used causing respective alterations to the governing Navier-Stokes equations. Consequently a new term accounting for internal friction effects, $...+\nabla\cdot\boldsymbol{\tau}*/\bar{\rho}$ is introduced with discrete particle notation (Gómez-Gesteira et al., 2007) in Eq. 5, involving the SPS stress tensor **τ*** in the likes of LES-SGS models

$$\boldsymbol{\tau}_{ij}^{*} = \bar{\rho}\left(2\nu_t \tilde{\mathbf{S}}_{ij} - \frac{2}{3}\tilde{k}\delta_{ij} - \frac{2}{3}C_I \Delta l^2 \delta_{ij} \left|\tilde{\mathbf{S}}_{ij}\right|^2 \right) \tag{10}$$

where C_I = 0.0066, Δl = inter-particle spacing, $\left|\tilde{\mathbf{S}}_{ij}\right| = \left(2\tilde{\mathbf{S}}_{ij}\tilde{\mathbf{S}}_{ij}\right)^{1/2}$, $\mathbf{S}_{ij}$ = the strain tensor

$$\tilde{\mathbf{S}}_{ij} = -\frac{1}{2}\left(\frac{\partial \tilde{\mathbf{u}}_i}{\partial x_j} + \frac{\partial \tilde{\mathbf{u}}_j}{\partial x_i} \right) \tag{11}$$

The eddy viscosity assumption (Boussinesq hypothesis) is currently employed in the framework of a standard Smagorinsky-type model (Smagorinsky, 1963) for the derivation of turbulent eddy viscosity as $\nu_t = [\min(C_s \Delta l)]^2 |S_{ij}|$, where the Smagorinsky coefficient C_s = 0.12. The former approach gives rise, using Eq. 10, to the ultimate SPS stress tensor symmetric formulation (Lo & Shao, 2002), in discrete notation:

$$\frac{1}{\rho}\nabla_i \tau_{ij}^{*} = \sum_j m_j \left(\frac{\tau_i^{*}}{{\rho_i}^2} + \frac{\tau_j^{*}}{{\rho_j}^2} \right) \cdot \nabla_i W_{ij} \tag{12}$$

To avoid unphysical results like secondary bumps on the free surface, unfortunately induced by the SPS stress treatment, Panizzo (2004) proposed the use of Shepard density averaging filter to ensure smoothness of free surface depiction and physicality of results, just as the XSPH approach (Eq. 7) averages the local velocities terms. The

filtering process is performed every 30-40 time steps, introducing re-initialisation of each water particle density, while allowing simultaneous detailed representation of the highly nonlinear processes of wave breaking, like plunging, overturning, splash-ups and wave impact, according to:

$$\rho_i = \sum_j m_j W_{ij} \Big/ \sum_j \frac{m_j W_{ij}}{\rho_j} \tag{13}$$

Numerical Schemes

Two numerical schemes are available in the SPHysics code, namely a Predictor-Corrector and the Verlet algorithm (Gómez-Gesteira et al. 2007, Verlet 1967). The time step is kept constant and small enough to ensure the fulfilment of the Courant criterion, although a variable time step option is also accessible. In general, the total energy is conserved within Monaghan (1994) proposed limits, with 0.1% energy loss over 400 time steps, as stated by the original authors of the code.

Special Features Calibration

In all our computations the Predictor-Corrector scheme was used together with repulsive Lennard-Jones forces for the solid boundary conditions. The spatial discretization spacing was $dx = dz = 0.02$m horizontally and vertically and the time step $dt = \sim 10^{-4}$ sec. The simulations were performed only in 2-D and the smoothing length coefficient $c_f = 0.92$, where $h = c_f (dx^2+dz^2)^{1/2}$.

The geometric and hydraulic features of the experiment used as input data [S&F] for the numerical wave tank simulations undertaken as validation of the SPHysics code are presented in Table 1. Specifically the horizontal distances of the gauges from the wave-maker boundary position are also given in Table 2. Further detailed description of the experimental setup can be found in their paper.

Table 1. Wave Flume Characteristic Features

Experiment	Water Depth d, m	Horizontal Distance l_x, m	Vertical Distance l_z, m	Bottom Slope	Wave Height H, m	Period T, sec	Breaker Type
S&F	0.34	11	0.6	0.05	0.105	2.42	Spil/Plung

Table 2. Gauges Horizontal Positions for Stansby & Feng (2005)

GAUGE	1	2	3	4	5	6	7	8	9	10
x (m)	1.1	2.4	3.4	3.9	4.4	4.9	5.3	5.54	5.6	5.74
GAUGE	11	12	13	14	15	16	17	18	19	20
x (m)	5.88	5.96	7.2	7.6	6.18	6.2	6.26	6.34	6.42	6.6
GAUGE	21	22	23	24	-	-	-	-	-	-
x (m)	6.8	7.1	7.2	7.6	-	-	-	-	-	-

MODEL VALIDATION, RESULTS & DISCUSSION

Characteristic results of the SPHysics implementation are provided in Fig. 1. The free-surface elevation pattern is portrayed by a reasonable undular form, with wave breaking in an obvious spilling form, which transforms into a weak plunging one in the inner surf zone. Particle discretization is obvious in Fig. 1b, where blank regions are not voids, but areas occupied by Lagrangian particles at other simulation time steps. An

unaccounted for discrepancy at the coast boundary depicted in Rogers & Dalrymple (2004) is still present in our simulations, probably due to excessive repulsion in solid boundary conditions. A streaming sequence of the instantaneous mappings of the output results reveals a weak plunging incident just as reported by the authors of the experimental research paper, allowing good qualitative agreement.

Acceptable quantitative plausibility, between experimentally and numerically derived wave heights, can also be seen by examining Fig.2, for the pre-breaking and the inner surf-zone regions. Disagreement of the wave height results can be traced at the intermediate gauges, where the model reveals an apparent over-diffusive behaviour, forcing the waves to an early spilling-type breaking situation. On the contrary, the mean surface elevation (wave setup) is very well predicted by the model.

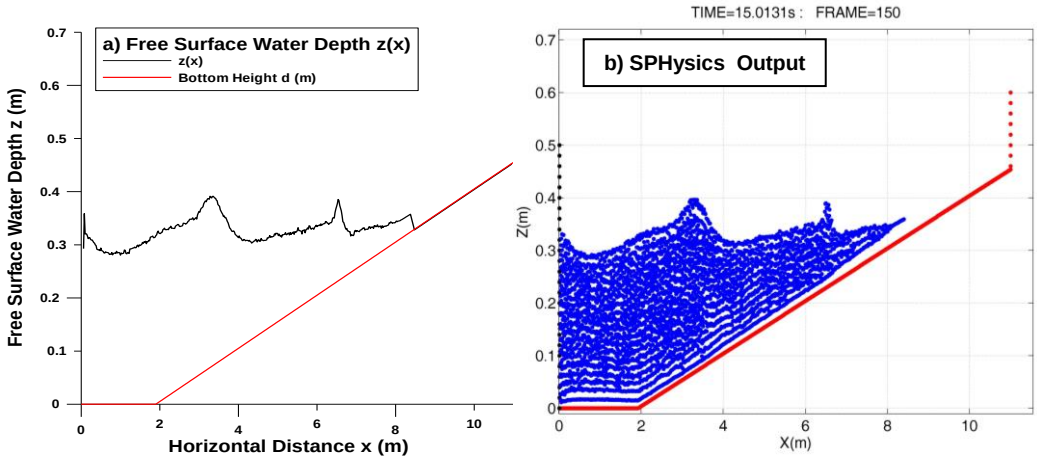

Fig. 1. SPHysics numerical results for S&F experimental setup at approx. t=15sec of the simulation: a) Free surface elevation b) SPHysics output

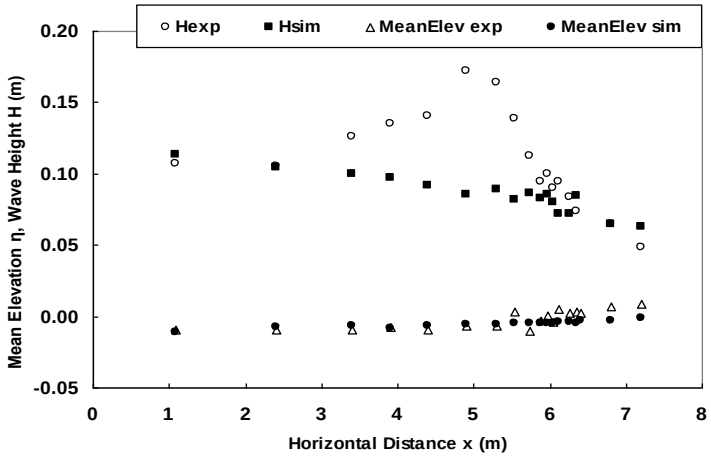

Fig. 2. Wave height 'H' and setup 'MeanElev' comparison between SPHysics simulation and S&F experiment

In Fig. 3, the ensemble-averaged free-surface elevation distributions (Nadaoka et al., 1989) are presented by our SPH simulations (red long dash) and S&F depth-integrated

shallow-water RANS equations results (blue short dash). The black line distribution corresponds to a typical instantaneous free surface profile in our simulations. The phase-lag between experimental and simulation results are of the order of 1~3%, which is minimal compared to the phase differences reported elsewhere, e.g. in SPH dam break wave evolution problems. The peak and trough drawdown is of the order of 0~40% and 2~30% respectively. In general there is apparent discrepancy in the incipient breaking region (e.g. gauges 8, 10), while in the inner surf zone (e.g. gauges 21, 23) the peak and trough drawdown cancel each other out revealing a good estimation of the wave height predicted by the SPHysics model with a minor difference in mean elevation values.

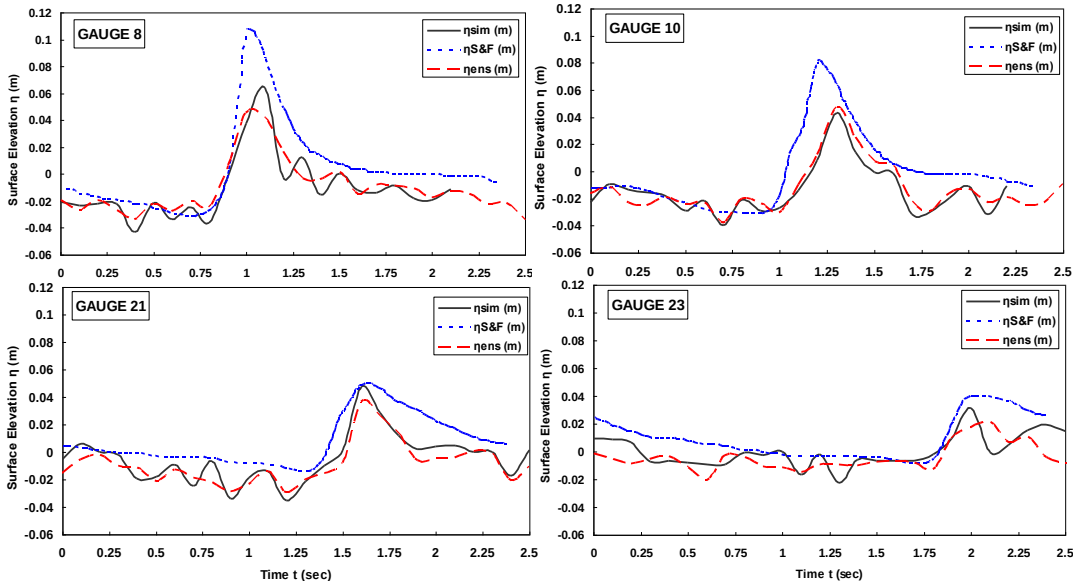

Fig. 3. Comparison of ensemble-averaged free surface elevation at gauges 8, 10 (incipient breaking region) and 21, 23 (inner surf zone)

The instantaneous velocity vector field is shown in Fig. 4, revealing the counter-directional character of the flow below the crest and trough and moreover the obliquely descending particle motion hind-ward of the breaking splash-up and the following bore propagation in the inner surf zone. Dalrymple (2006) mentions probably similar obliquely descending eddy formation detected in 3-D SPHysics simulations. The vertical motion of the fluid particles under the turbulent bore in the swash-zone, which becomes nearly horizontal in the bore front, is also obvious, as well as the maximum celerity being of the order 70~80% of the theoretical value for shallow water, $c_t = (gd)^{1/2}$.

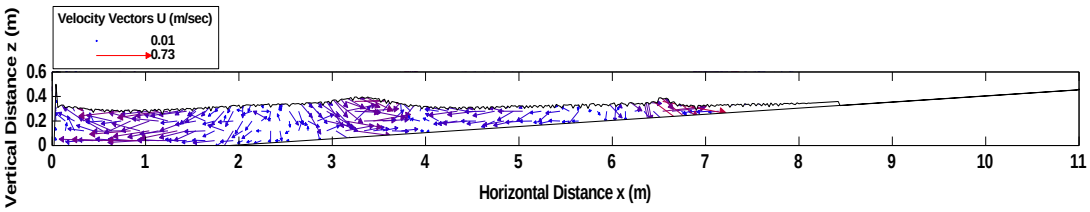

Fig. 4. Instantaneous velocities vector plot at approx. t=15sec

Fig. 5 presents the comparison between our and S&F simulations for the depth- and ensemble-averaged velocities at the same as before gauges. Similar distribution patterns are detected with smaller values for our results, due to the fact that the predicted wave amplitudes at the specific gauges in our simulations are smaller than those of the experiment and the S&F simulations.

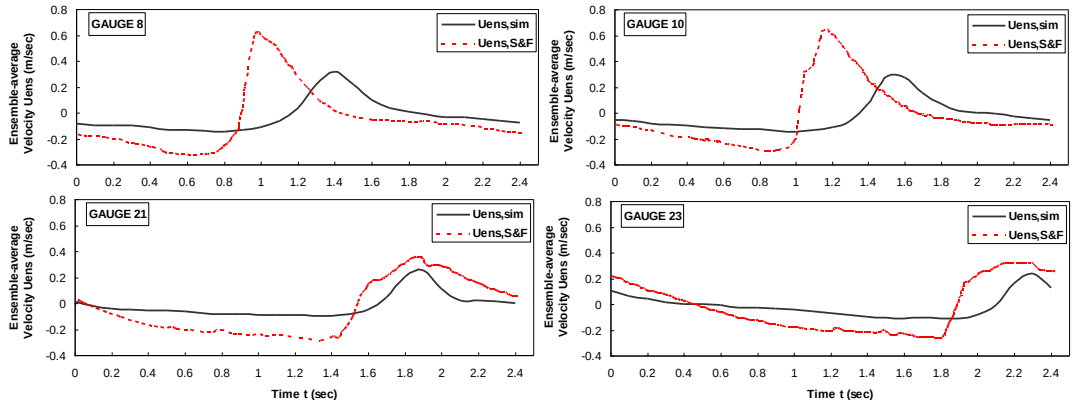

Fig. 5. Comparison of ensemle-averaged velocities at gauges 8, 10 (incipient breaking region) and 21, 23 (inner surf zone)

Another interesting feature is presented in Fig. 6. The time-averaged, vertically distributed numerical values of the velocity vectors are shown at various gauges covering the whole of the surf zone, allowing us to clearly distinguish the undertow trend below the mean elevation from the near-surface net mass transport (Stokes drift). The shear interface, in-between the two, is spotted at around the wave setup level, while the calculated trough envelope, based on wave amplitude, is located at z = 0.29m. Characteristic values of depth-averaged undertow velocities are given in Table 3, with a seaward mean around 0.02m/sec, whereas the shoreward depth-averaged Stokes drift velocity fluctuates from 0.27m/sec, in the region near the breaking point, to 0.55 m/sec and 0.35m/sec in the inner surf zone and the swash zone respectively.

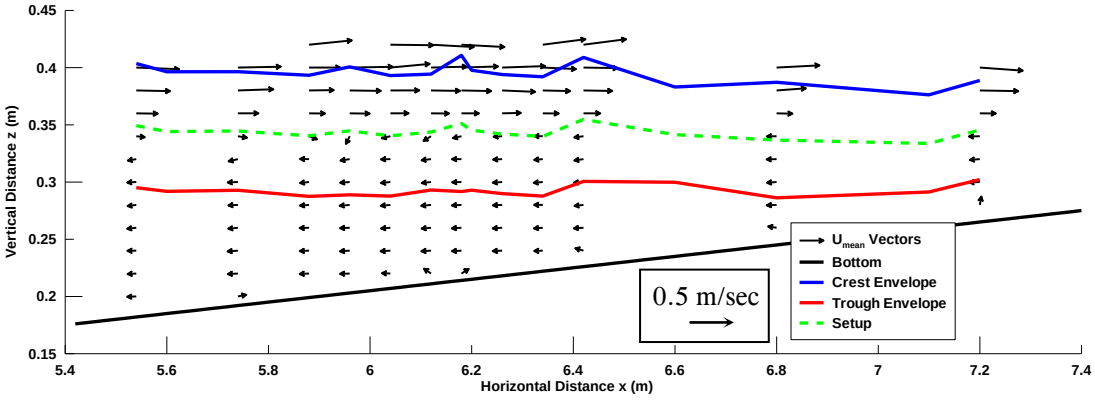

Fig. 6. Time-averaged vertical distribution of velocity vectors at various gauges (8, 10-15, 17-19, 21, 23) covering the whole surf zone

Table 3. Depth-averaged undertow velocities Ū (m/sec)

GAUGES	8	10	11	12	13	14
Ū	0.022	0.018	0.021	0.019	0.017	0.016
GAUGES	15	17	18	19	21	23
Ū	0.016	0.019	0.021	0.019	0.023	0.021

Vertical profile distributions of the time-averaged horizontal velocities $\bar{\mathbf{u}}$ and vorticity $\bar{\boldsymbol{\omega}}$ at the same gauges are given in Fig. 7, where the vorticity $\boldsymbol{\omega}$ can be derived from the following equation, written in discrete notation (Crespo et al., 2008):

$$\boldsymbol{\omega} = \vec{\nabla} \times \mathbf{u} = \sum_j m_j \left(\mathbf{u}_i - \mathbf{u}_j \right) \times \nabla_i W_{ij} \tag{14}$$

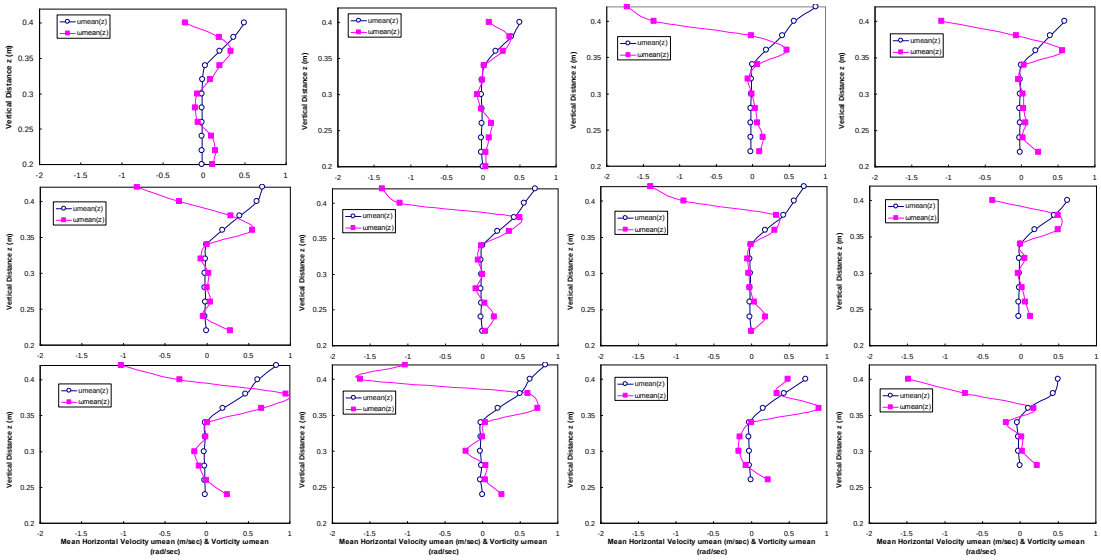

Fig. 7. Time-averaged vorticity (magenta square) and horizontal velocity (blue circle) vertical distributions at various gauges (8, 10-15, 17-19, 21, 23, from left to right)

We can note that the calculated vorticity gradient near the surface at gauges placed in the initial breaking region are far smaller than the respective one at gauges in the mid and inner surf zone, where elongated cross-shore turbulent structures are probably created. This fact can be defined by measurable lateral vorticity (Christensen, 2006), not yet available in our analysis due to lack of 3-D effects. The above comparison indicates enfeeblement or even lack of plunging jet formation and consequent overturning and splash-up by an impinging jet on the forward trough. The latter constitutes the main mechanism of vorticity generation and enhancement due to turbulent production in wave breaking. The lack of it is visually verified in the incipient breaking region. On the contrary, weak plunging is visually traceable, as mentioned, in the inner surf zone region, where the vorticity vertical gradients become important, in terms of numerical results (gauges 11-23, Fig. 7). The most probable cause for this discrepancy is the Smagorinsky-type model consideration of the C_s factor which is kept constant and equal to 0.12 throughout the whole computational domain, not taking into account the

velocity vector field evolution and its spatial gradients. We therefore propose the use of a dynamic Smagorinsky-type model, based on the similarity concept and Germano's identity (Germano et al. 1991, Lilly 1992) for further research. Moreover the comparison of flow properties, derived by SPH simulations, such as k, u', w', τ' as well as both the macroscopic length, velocity and time scales, the inertial intermediate scales and the Taylor and Kolmogorov micro-scales, against data from other experiments, is being prepared for future investigation.

Another important concern, for the application of the SPHysics code to practical cases, is related to affordable computational time and adequate spatial discretization depending on each other according to the Courant criterion for numerical stability. Preliminary results of the same simulations with smaller dx than 0.01m show better depiction of the plunging-type breaking and larger accuracy in results, yet the computations crash more easily and the computational time becomes 10 to 20 times longer, nearly unaffordable for classic scalar simulations. New parallel versions of the code soon to be released are expected to somehow address this issue.

CONCLUSIONS

The modern promising mesh-free numerical method SPH is being used for the simulation of wave propagation and breaking. A SPS Smagorinsky-type eddy viscosity model is used for the closure of turbulence, accounting for shear friction forces leading to turbulent energy dissipation in the unresolved scales by the model, resembling the Sub-Grid Scale approaches incorporated in Large Eddy Simulation models. The 'open source' academic code SPHysics (Gómez-Gesteira et al., 2007) is being implemented and expanded with new subroutines transforming the Lagrangian output of the model to Eulerian. The derived data are being tested against the experimental ones by Stansby & Feng (2005) and fairly good agreement is achieved, in terms of ensemble-averaged free-surface elevation and velocities. The predicted wave height is plausible for the pre-breaking and inner surf zones, yet the wave breaking process is somehow overestimated in the incipient and mid breaking region, resulting in underestimation of wave height there. Vertical profiles of vorticity indicate that the Smagorinsky constant used in the present analysis is insufficient in determining the turbulent energy cascade from the inertial to the microscopic scales. Further turbulent velocity spectral analysis and determination of the turbulent kinetic energy in the various scales should enlighten the matter. The use of a dynamic Smagorinsky-type model, based on Germano's identity (Germano et al. 1991, Lilly 1992) and taking into account, the spatial derivatives of the surrounding velocity field, is proposed for future research. In addition, the undertow and near-surface mass transport were investigated, with good qualitative performance by the SPHysics model. Further calibration of the SPHysics model in terms of spatial discretization and boundary conditions, as well as the implementation of 3-D simulations, are expected to yield even better results.

REFERENCES

Batchelor, G.K. (1974). "*Introduction to Fluid Dynamics*", Cambridge Univ. Press.

Christensen, E.D. (2006). "Large eddy simulation of spilling and plunging breakers", *Coastal Engineering*, 53, 463-485.

Crespo, A.J.C., Gómez-Gesteira, M., and Dalrymple, R.A. (2007). "3D SPH simulation of large waves mitigation with a dike", *J. Hydr. Res.*, 45(5), 631-642.

Crespo, A.J.C., Gómez-Gesteira, M., Narayanaswamy, M.S., and Dalrymple R.A. (2008). "A hybrid boussinesq-SPH model for coastal wave propagation", *Proc. 3rd SPHERIC Workshop*, ERCOFTAC, 4-6 June, Lausanne, Switzerland.

Dalrymple, R.A. (2006). "Smooth Particle Hydrodynamics for Surf Zone Waves", Tcnical Report Web Summary, http://www.onr.navy.mil/sci_tech/32/reports/docs/06/cgdalrym.pdf

Dalrymple, R.A., and Rogers B.D. (2006). "Numerical modeling of water waves with the SPH method", *Coastal Engineering*, 53(2-3), 141-147.

Elfrink, B., and Baldock, T. (2002). "Hydrodynamics and sediment transport in the swash zone: a review of perspectives", *Coastal Engineering*, 45(3-4), 149-167.

Germano, M., Piomelli, U., Moin, P., and Cabot W.H. (1991). "A dynamic subgrid-scale eddy viscosity model", *Phys. Fluids A*, 3(7), 1760-1765.

Gómez-Gesteira M., Rogers, B.D., Dalrymple, R.A., Crespo, A.J.C., and Narayanaswamy, M. (2007). "User guide for the SPHysics code", http://wiki.manchester.ac.uk/sphysics/images/SPHysics_v1.2.000_GUIDE.pdf

Grue, J., Liu, P.L.F., and Pedersen, G.K. [Editors] (2004). "PIV and water waves", *Advances in Coastal & Ocean Engineering*, 9, World Scientific Publishing.

Lilly, D.K. (1992). "A proposed modification of the Germano subgrid-scale closure method", *Phys. Fluids A*, 4(3), 633-635.

Liu, G.R., and Liu, M.B. (2003). "*Smoothed Particle Hydrodynamics, a meshfree particle method*", World Scientific Publishing.

Lo, E., and Shao, S. (2002). "Simulation of near-shore solitary wave mechanics by an incompressible SPH method", *Applied Ocean Research*, 24, 275-286.

Longo, S., Petti, M., and Losada, I.J. (2002). "Turbulence in swash and surf zones: a Review", *Coastal Engineering*, 45(3-4), 129-147.

Monaghan, J.J. (1994). "Simulating free surface flows with SPH", *J. Comp. Phys.*, 110, 399-406.

Monaghan, J.J. (2005). "Smoothed Particle Hydrodynamics", *Rep. Prog. Phys.*, 68, 1703-1759.

Nadaoka, K., Hino, M., and Koyano, Y. (1989). "Structure of the turbulent flow field under breaking waves in the surf zone", *J. Fluid Mech.*, 204, 359-387.

Panizzo, A. (2004). "*Physical and numerical modeling of subaerial landslide generated waves*", PhD Dissertation, Universita Degli Studi di L'Aquila, Italy.

Rogers, B.D., and Dalrymple, R.A. (2004). "SPH modeling of breaking waves", *Proc. 29th ICCE*, World Scientific Press, 415-427.

Smagorinsky, J. (1963). "General circulation experiments with the primitive equations: I. The basic Experiment", *Monthly Weather Review*, 91, 99-164.

Stansby, P.K., and Feng, T. (2005). "Kinematics and depth-integrated terms in surf zone waves from laboratory measurement", *J. Fluid Mech.*, 529, 279-310.

Verlet, L. (1967). "Computer experiments on classical fluids: I. Thermodynamical properties of Lennard– Jones molecules", *Phys. Rev.*, 159, 98-103.